Supplementary Information

Metal Oxide Resistive Memory with a Deterministic Conduction Path

*Sunghwan Lee, Shem Seo, Jinho Lim, Dasom Jeon, Batyrbek Alimkhanuly, Arman Kadyrov, Seunghyun Lee**

Semiconductor Device & Integration Laboratory, Department of Electronic Engineering, Kyunghee University, 17104, Rep. of KOREA

*Corresponding author. E-mail: seansl@khu.ac.kr

S1. Arrhenius type plot of the wait time versus 1/T extracted from Fig. 2e.

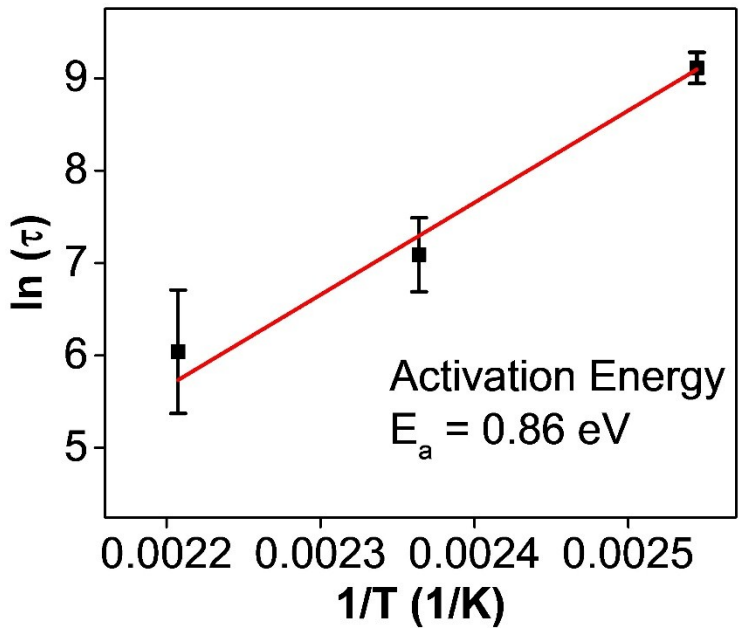

Fig. S1. Arrhenius type plot of the wait time versus 1/T extracted form Fig. 2e.

The sudden transitions to the OFF state in Fig. 2e correspond to the rupture of the oxygen vacancy-based filament owing to the diffusion of oxygen ion toward the HfO_2 layer. The activation energy of the barriers can be extracted from temperature dependence of the characteristic dwell time for the RESET transition. From the linear fitting of retention time in logarithm scale versus reciprocal temperature, we estimated the activation energy E_a for ion migration in the Ge–Sb–Te layer to be 0.86 eV.

This measurement can probe the thermal activation of oxygen ion migration, as shown in Fig. 2e. The elevated temperature was utilized to obtain the critical time (i.e., filament rupture time) for oxygen migration within a reasonable time frame. This will cause the oxygen ions to migrate back to HfO_2, thus increasing the resistance of the RRAM. The kinetics of this process can be described using the Arrhenius law as follows:

$$\tau_{reset} = \tau_0 \cdot e^{\frac{E_a}{k_B T}},$$

where τ_{reset} is the characteristic time for the RESET transition, τ_0 is a constant, k_B is the Boltzmann constant, E_a is the activation energy barrier, and T is the absolute temperature. The linear fitting result of the retention time in logarithmic scale versus reciprocal temperature provides a good estimation of the activation energy (Fig. S1, Supplementary Information).

S2. Pulse conditions for the endurance tests of both stand-alone RRAM and RRAM with GeSbTe

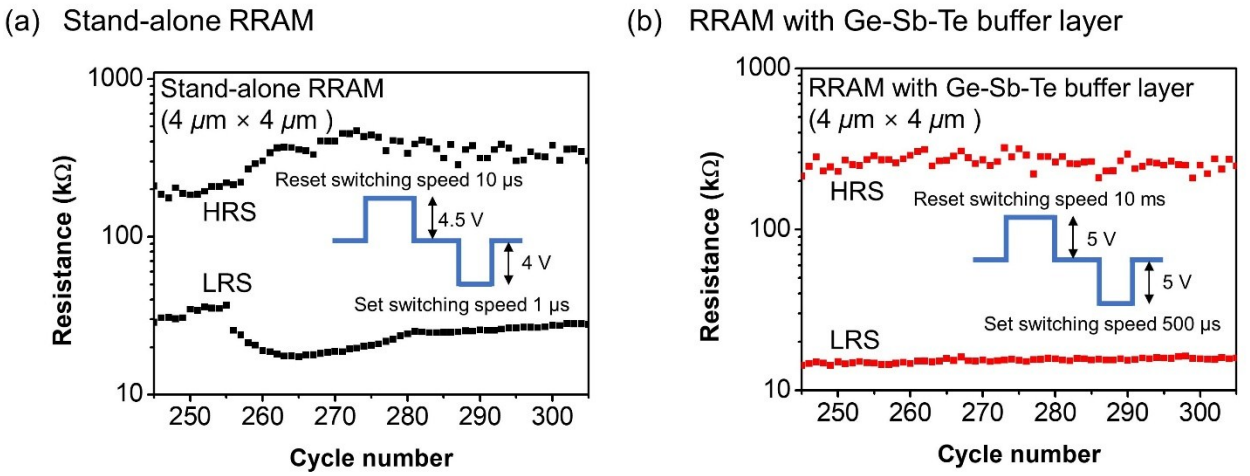

Fig. S2. Pulse measurement conditions (single pulse only for consecutive switching) of stand-alone RRAM and RRAM with the buffer layer. Increased pulse strength and time is required for (b) due to added buffer layer.

S3. Characteristics of Ge-Sb-Te chalcogenide material.

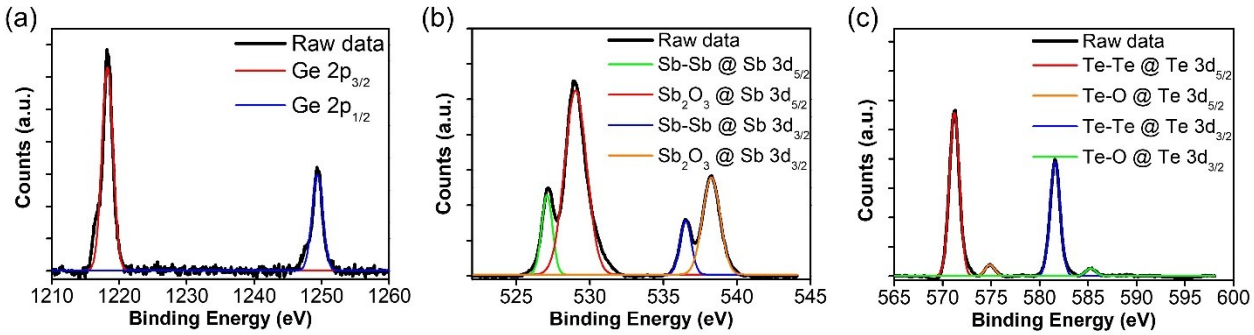

Fig. S3. XPS spectra of (a) Ge 2p, (b) Sb 3d, and (c) Te 3d formed via RF sputtering. Black solid line represents the raw data, and the colored solid lines represent each component of Ge 2p, Sb 3d, and Te 3d.

Material characteristics and binding states of Ge, Sb, and Te in the chalcogenide film are observed via X-ray photoelectron spectroscopy (XPS), as shown in Fig. S2. Fig. S2a shows the XPS spectra of Ge 2p. Ge $2p_{3/2}$ shows a peak at 1218.28 eV, whereas Ge $2p_{1/2}$ shows a peak at 1249.28 eV. Ge $2p_{3/2}$ with a peak of 1218.28 eV is attributed to the Ge–Sb or Ge–Te metallic bond, not to the Ge–Ge bond, with Ge–Sb–Te layer sputtering at room temperature[1–4]. Fig. S2b shows the XPS spectra of Sb 3d. Sb $3d_{5/2}$ shows peaks at 527.18 and 528.98 eV, whereas Sb $3d_{3/2}$ shows peaks at 536.48 and 538.28 eV. The peaks, i.e., 527.18 eV of Sb $3d_{5/2}$ and 536.48 eV of Sb $3d_{3/2}$, exhibit a Sb–Sb homo-polar bond. In contrast, the peaks, i.e., 528.98 eV of Sb $3d_{5/2}$ and 538.28 eV of Sb $3d_{3/2}$, form Sb_2O_2 via the Sb–O bond due to strong surface oxidation effects. Consequently, the Sb–O bond shows a stronger peak than the Sb–Sb homo-polar bond[2,3,5]. Fig. S2c shows the XPS spectra of Te 3d. Te $3d_{5/2}$ shows peaks at 571.68 and 574.78 eV, whereas Te $3d_{3/2}$ shows peaks at 581.98 and 585.38 eV. The peaks with the Sb–Te and Te–Te metal bonds are located at 571.68 eV of Te $3d_{5/2}$ and 581.98 eV of Te $3d_{3/2}$, whereas those at 574.78 eV of Te $3d_{5/2}$ and 585.38 eV of Te $3d_{3/2}$ represent the Te–O bonds[2,3,5].

REFERENCES

1 L. Shen, S. Song, Z. Song, L. Li, T. Guo, Y. Cheng, S. Lv, L. Wu, B. Liu and S. Feng, *Appl. Phys. A Mater. Sci. Process.*, 2016, **122**, 2–7.

2 T. Wei, J. Wei, K. Zhang, H. Zhao and L. Zhang, *Sci. Rep.*, 2017, **7**, 1–7.

3 H. Y. Cheng, C. A. Jong, R. J. Chung, T. S. Chin and R. T. Huang, *Semicond. Sci. Technol.*, 2005, **20**, 1111–1115.

4 Z. Zhang, J. Pan, L. W. W. Fang, Y. C. Yeo, Y. L. Foo, R. Zhao, L. Shi and E. S. Tok, *Appl. Surf. Sci.*, 2012, **258**, 6075–6079.

5 W. S. Lim, S. J. Cho and H. Y. Lee, *Thin Solid Films*, 2008, **516**, 6536–6540.